COMMUNICATION

Graphene Oxide Nanoribbon Assembly toward Moisture-Powered Information Storage

Fei Zhao, Lixia Wang, Yang Zhao, Liangti Qu, and Liming Dai**

Ion migration across biomembranes is ubiquitous in natural organisms and can induce a bioelectric potential to mediate various biochemical processes in cells or tissues. One of the well-known examples is the bioelectric potential in neurons of the human brain for information record, where the biochemical energy was converted to electric power to achieve the memory function.[1,2] The key for translating the biological information storage into practical application is to efficiently imitate this bioelectric potential in neuron, which has been precluded by the complex microstructure of human neurons. Nevertheless, recent effort has uncovered that similar "memory process" in the bacteria could be derived from a porous layered structure of peptidoglycan with switchable ion channels for a gradient ion distribution.[3] Although this biochemical energy-powered "memory process" depends strongly on living systems and can hardly work in ambient environments.[4–6] The discovery of this simple porous functional structure opens up new opportunities for the development of artificial self-powered devices, which integrate power generation and unique functions of certain biological tissues.

Information storage has also been achieved by specially designed electronic systems outside the biological organisms. In this context, memory diode is a typical advanced information storage device. However, despite the advantages such as low error risk, low cost and easy to prepare, obvious drawbacks, including the producing of intense heat (also the reason why specially designed heat dissipation system is necessary for almost every kinds of modern electronic in our life) and the dependence of complex power supply system, severely limited their general acceptability, operational reliability, and safety.[7,8] Recently, several strategies have been devised to produce new materials and/or structures, which can reclaim the electrothermal energy to improve the performance of memory diodes, for equivalent weakening the self-heating effect.[9–12] Meanwhile, great effort has also been made to develop updated data storage technologies that were assisted by other energy resources such as light,[13] force,[14] and heating (or cooling),[15] attempting to simplify the corresponding power supply system. However, the memory diodes reported so far still rely on the external power supply, which have to afford the considerable energy consumption of electrothermal effect. Therefore, self-powered memory devices without self-heating are highly desired.

Herein, we developed a novel bioinspired micromembrane by stacking graphene oxide nanoribbon (GOR) networks (GOR-Ns) into layered GOR-N membrane (GOR-NM) through dimensionally confined freezing self-assembling[16,17] for self-powered potential switching memory. The GORs were specifically chosen in this work because they were enriched with oxygen-containing hydrophilic functional group (**Figure 1**a) and could form widely distributed nanopores running through the GOR-NM (Figure 1b,c), which could not only accelerate the moisture capture, but also largely facilitated the ion transportation, hence enabling efficient writing and reading process. The formed nanomeshes in each network layer (Figure 1b) are connected as ion channels through the membrane thickness. Subsequent water molecule filling through hydration process could lead to an enhanced ion transport, and hence switching on the ion channels (Figure 1c). By rendering the GOR-NM with an oxygen functional group gradient (designated as: gradient GOR-NM, g-GOR-NM) via electrochemical reduction on one side of the member and oxidation on the other (vide infra), the captured water could trigger an ion concentration gradient, leading to a potential switchable g-GOR-NM with both opened ion channels and ion concentration gradient upon exposure to the moisture (Figure 1d). As we shall see later, this moisture enabled potential switching with g-GOR-NM sets the basis for the development of breath (self-)powered write-once-read-many-times (WORM)-type memory devices with an excellent flexibility, reliability, and superior ON/OFF voltage ratio of up to 10^6.

The GOR was prepared by longitudinal unzipping of multi-walled carbon nanotubes (MWCNTs) through an oxidizing reaction (see Figure S1, Supporting Information, for details).[18] The resultant GORs were then used to prepare the layered GOR-NM by the dimensionally confined freezing self-assembling under a cold source fixed to one side of a microcontainer sheathed with thermal baffles (see Figure S2, Supporting Information, for details), in which the crystalline ice formed during freezing can serve as template for the assembly of dispersed GORs by expelling them to the boundaries of adjacent ice crystals.[19,20] Owing to the directional growth of ice crystals caused by the unilateral cold source, the assembly of GORs is confined to be oriented (also see Figure S3, Supporting Information, for control sample

Dr. F. Zhao, Dr. L. Wang, Dr. Y. Zhao, Prof. L. Qu
Beijing Key Laboratory of Photoelectronic/Electrophotonic Conversion Materials
Key Laboratory of Cluster Science
Ministry of Education
School of Chemistry
Beijing Institute of Technology
Beijing 100081, P. R. China
E-mail: lqu@bit.edu.cn
Prof. L. Dai
Center of Advanced Science and Engineering for Carbon (Case 4Carbon)
Department of Macromolecular Science Engineering
Case School of Engineering
Case Western Reserve University
10900 Euclid Avenue, Cleveland, OH 44106, USA
E-mail: liming.dai@case.edu

DOI: 10.1002/adma.201604972

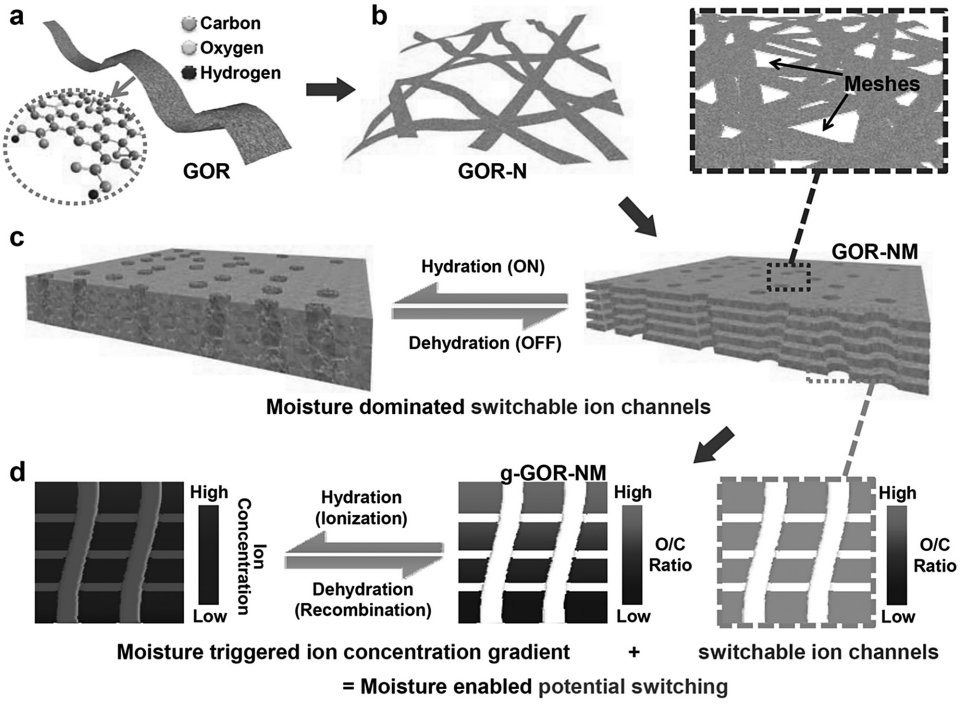

Figure 1. Synthetic strategy for an artificial moisture-enabled potential switching. a) The GORs that contain plenty of oxygen-containing groups are assembled into b) planar networks (GOR-Ns). c) The GOR-Ns are further stacked together to form a GOR-N membrane (GOR-NM), where the formed meshes connect as channels across the membrane. These ion channels can be turned ON and OFF by hydration and dehydration process, respectively. d) When the uniform distribution of oxygen-containing groups in the GOR-NM is regulated to be gradient, the ionization of these groups leads to an ion concentration gradient, which can be eliminated by recombination of anions and cations. The ionization and recombination can be triggered by hydration and dehydration process, respectively. Combining the moisture switchable ion channels and ion concentration gradient, a moisture dominated potential switching is achieved for self-powered information storage (not drawn to scale).

from the free-growth process). Subsequent freeze drying sublimated the ice and gave rise to an aerogel consisting of layer-by-layer organized GOR-Ns (i.e., GOR-NM).

Figure 2a,b reproduces a typical scanning electron microscope (SEM) cross-section image of an as-prepared GOR-NM with ≈20 layers of GOR-Ns, which shows that GOR-Ns are well oriented in a nearly parallel manner with a controlled layer number (see Figure S4, Supporting Information, for details). The top view of GOR-NM (Figure 2c) presents a continuous weaving structure of GORs with meshes of a size ranging from tens nanometers to several micrometers (Figure 2d). The transmission electron microscopic (TEM) imaging (Figure 2e,f) confirms the presence of widely distributed nanopores with diameters of ≈100 nm (dashed circles) within the GOR-NM.

X-ray photoelectron spectrum (XPS, Figure S5, Supporting Information) of GOR-NM shows an oxygen/carbon (O/C) atomic ratio of ≈0.45, indicating the enrichment of oxygen-containing hydrophilic functional groups within the GOR-NM. The high resolution C 1s spectrum (**Figure 3**a) reveals three oxygen-related peaks at 286.6, 288.5, and 289.5 eV, corresponding to the C—O bonds (hydroxy), C=O bonds (carbonyl) and HO—C=O bonds (carboxyl), respectively.[21,22] These polar functional groups can not only accelerate the moisture capture but also facilitate the ion transportation.[23] The capability of GOR-NM for capturing moisture was evaluated by the saturated water content and corresponding elapsed time under various environmental humidity (Figure 3b). The saturated water content was determined by dividing the weight of trapped water (m_w) by the weight of hydrated GOR-NM (m_h), where the m_w equals to m_h minus the weight of original GOR-NM (m_0). As can be seen in Figure 3b, the saturated water content increased with increasing environmental relative humidity (RH) up to 57% at RH of 90%. The initial hydration of GOR-NM was rapid due to the synergy of hydrophility and capillarity.[24,25] Further adsorption of water took a relative long period of time, attributable to the reduced capillarity caused by partial hydration (see Figure S6, Supporting Information, for control experiment with beforehand weakened capillarity). To study the hydration process in a more quantitative manner, a hydration efficiency factor was defined as the ratio of the saturated water content to the elapsed time (Figure S7, Supporting Information). The most efficient hydration was found at RH = 35%. On the other hand, the resistance test can serve as real-time monitoring for the switching of ion channels in GOR-NM as previous studies have demonstrated that the switching of ion channels caused changes in resistance of the macroscopic assembly.[26] As shown in Figure 3c (blue curve), the resistance of GOR-NM rapidly reduced once the environmental RH changed from 5% to 35%, indicating a moisture induced switching-on of the ion channels. Meanwhile, the variation of water content can be real-timely monitored (Figure 3c, red curve). By plotting the water content as a function of the resistance, an inversely proportional relationship was obtained (Figure S8, Supporting Information), indicating an efficient hydration of GOR-NM.

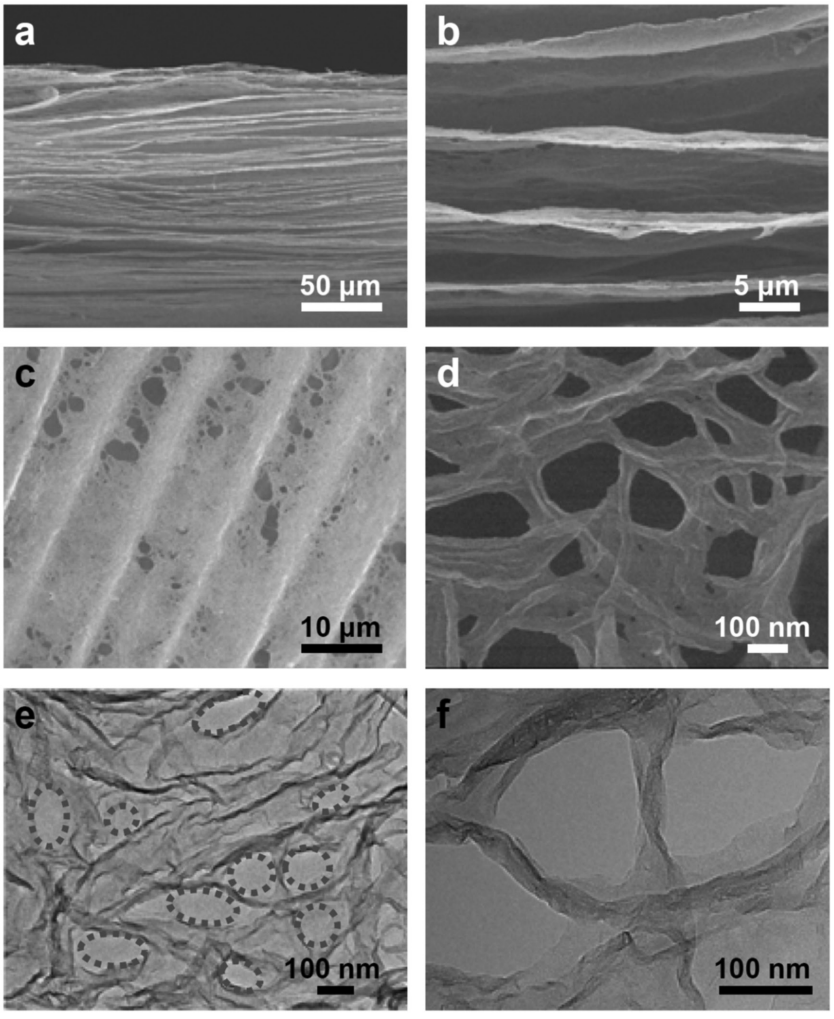

Figure 2. Structural characterization of GOR-NM. a,b) Typical cross-section and c,d) top-view SEM images of GOR-NM, showing the stacked structure of planar GOR-Ns with plentiful pores; e,f) TEM images of a single layer GOR-N with highlighted (dotted line) nanopores.

Furthermore, a half-saturated water adsorption period of ≈5 ms (from 247 to 252 ms) was observed (inset of Figure 3c), demonstrating an ultrafast hydration and excellent moisture sensitivity for the newly developed GOR-NM.

In the presence of water molecules, significant ionization of the polar functional groups within GORs occurred.[18] Indeed, the pH value of a GOR solution decreased with increasing GOR concentration (C_{GOR}, Figure 3d), indicating possibilities for GOR-NM to serve as a moisture triggered ion provider to enhance its ionic conductivity for mimicking the biological ion channels.[16] The variation of ionic conductivity with RH can be monitored by impedance measurements on the GOR-NM under various environmental RHs without the addition of any external electrolyte (see Figure S9, Supporting Information, for details). It was found that the ionic resistance of a hydrated GOR-NM decreased by two orders of magnitude upon increasing RH from 5% to 35% (Figure 3e), indicating a remarkably increased ionic conductivity in GOR-NM during moisture-induced hydration. To investigate the moisture controlled ion channel switching, we collected the current signals of GOR-NM (5 mm × 5 mm) at a constant external voltage of 1 V with and without the application of 30% RH variation (ΔRH). Figure 3f clearly shows a typical switching behavior of ion channels with a high switching rate and good repeatability.[16]

The GOR has abundant oxygen-containing groups (e.g., carboxyl) and active defects (e.g., carbon on the edge), which could be electrochemically reduced and oxidized under reducing and oxidizing potential, respectively.[27–29] Thus, the structural polarization could be realized in a short period of time by simply contact of a GOR-NM with two opposite electrodes. Finally, the cathode side of GOR-NM can be reduced while the anode side is oxidized to produce a g-GOR-NM (Figure S10, Supporting Information). As shown in **Figure 4**a, the O/C atomic ratio of the obtained g-GOR-NM gradually decreases from region 1 to 5, demonstrating the gradient distribution of oxygen-related groups through the membrane thickness. Moreover, X-ray diffraction (XRD) patterns from the surfaces near to region 1 and 5 of g-GOR-NM (sign as 1-side and 5-side, respectively) exhibit a distinct peak shift (Figure 4b). Unlike the GOR-NM with a uniform interspacing of ≈0.8 nm, the 1-side of the g-GOR-NM shows a relatively larger calculated interspacing of ≈0.9 nm with respect to the corresponding value of ≈0.65 nm for the 5-side of the same membrane, reflecting the electrochemical oxidization to introduce more oxidized functional groups at the 1-side and partially reduction at the 5-side of the g-GOR-NM. The asymmetric electrochemical redox reactions were also confirmed by the XPS measurements on both sides of the g-GOR-NM, which show graphitic C 1s peak at ≈284 eV and O 1s peak at ≈532 eV (Figure S11, Supporting Information). As expected, the O/C atomic ratio for the 1-side of the g-GOR-NM is ≈0.58, which is slightly higher than that of the original GOR-NM (≈0.45), whereas the corresponding O/C atomic ratio for the 5-side (≈0.16) of the g-GOR-NM is much lower than that of the original GOR-NM (≈0.45), indicating, once again, the successful asymmetric electrochemical oxidation and reduction. Further insights on the chemical composition changes induced by the asymmetric redox process can be obtained from the curve-fitted high resolution C 1s spectra given in Figure 4c, which shows an enhanced C—O peak at ≈287 eV (Figure 4c, cf. Figure 3a) associated with the introduction of additional hydroxyl (and/or epoxy) groups by the electrochemical oxidation of the 1-side of the g-GOR-NM,[21] and a weakened C=O peak at 288.5 eV and HO—C=O peak at 289.5 eV (Figure 4c, cf. Figure 3a) due to the deoxidation of carbonyl and carbonyl groups by electrochemical reduction of the 5-side of the same membrane[22]). As a result, the gradient distribution of oxygen-containing groups

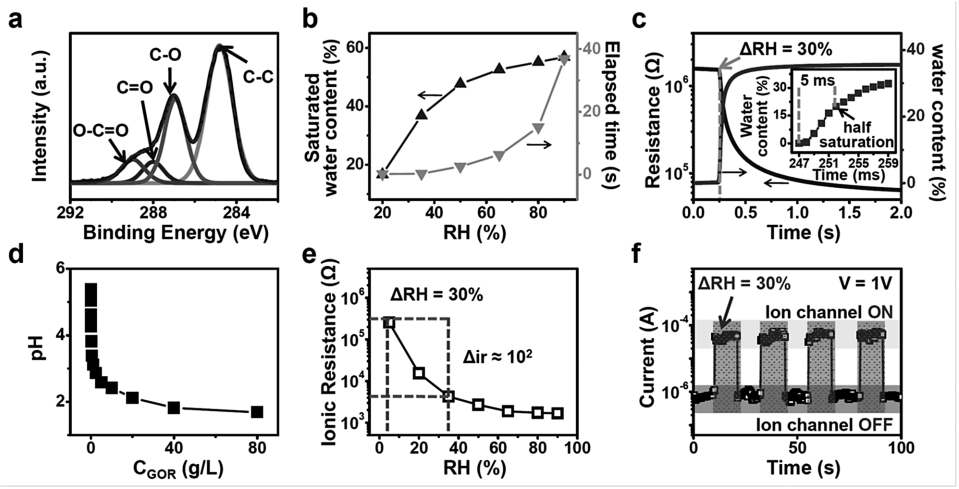

Figure 3. Demonstration of moisture-dominated switchable ion channels. a) High resolution C 1s XPS spectrum of GOR-NM. b) Saturated water content of GOR-NM and corresponding elapsed time under specific RH. c) Real-time monitoring of resistance and water content of GOR-NM upon ΔRH of 30%. Inset: High-resolution real-time monitoring of water content change, where a half saturation time of 5 ms is revealed. d) Dependence between pH value and GOR concentration (C_{GOR}). e) The ionic resistance change (Δir) with RH variation (ΔRH), where a Δir of ≈10^2 induced by ΔRH = 30% is presented. f) Current–time characteristics under applied voltage of 1 V and ΔRH = 30%, showing the distinct switch of ion channels controlled by moisture.

provides a moisture triggered ion gradient in g-GOR-NM. To investigate the self-powered moisture triggered ion gradient, we inserted the g-GOR-NM into a test circuit without power supply (Figure 4d). Upon hydration, the oxygen containing groups within the g-GOR-NM were ionized to produce free cations (H^+) and locally confined anions ($O^{\delta-}$, covalently bonding with GOR skeleton).[17] Due to the preformed gradient of oxygen-containing functional groups by the asymmetric electrochemical redox process described above, a gradient distribution of ion concentrations (C_{ion}) was formed within the hydrated g-GOR-NM. Consequently, the ion concentration gradient thus formed can boost the migration of free cations through the ion channels to induce potential switching on exposure of the g-GOR-NM to moisture. As shown in Figure 4e, the expected moisture-triggered voltage (≈40 mV) was observed when the RH increased from 5% to 35% within 0.2 s, indicating a higher response rate comparing with GO films.[17] Moreover, the moisture-induced voltage could support a short-circuit current of ≈0.3 mA cm^{-2} for 0.8 s with a ΔRH of 30% (Figure 4f). In addition, this unique moisture-triggered potential switching is highly reversible (Figure S12, Supporting Information) and free from capacitance effect (Figure S13, Supporting Information).

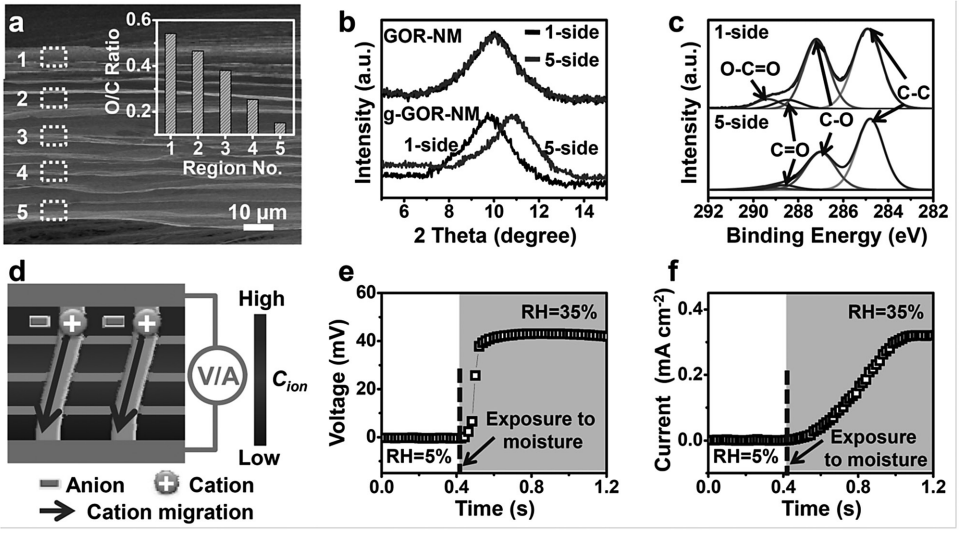

Figure 4. Demonstration of moisture-triggered ionic gradient. a) Cross-section SEM image with corresponding regional X-ray energy dispersive spectroscopy (EDS) analysis (inset). b) XRD patterns of different sides of the as-prepared GOR-NM and g-GOR-NM, where the surfaces near to regions 1 and 5 in (a) are noted as 1-side and 5-side, respectively. c) XPS spectra of different surfaces of g-GOR-NM. d) Schematic illustration of characterization strategy for ionic gradient in hydrated g-GOR-NM, where the blue channel represents opened ion channels. e) Open-circuit voltage and f) short-circuit current from directed migration of H^+ induced by moisture triggered ionic gradient in g-GOR-NM (ΔRH = 30%).

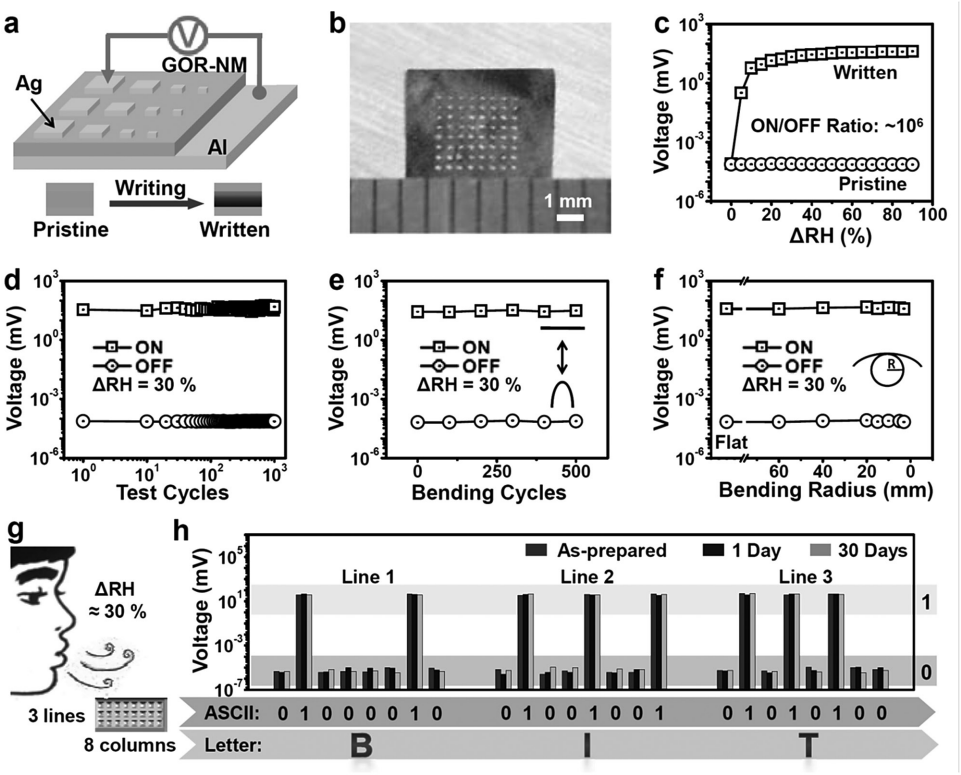

Figure 5. Moisture-powered WORM-type memory device based on GOR-NM. a) Schematic illustration and b) photograph of GOR-NM-based memory cell array. c) Collected signals from moisture-powered reading process with different ΔRH. d–f) Endurance and continuous bending test of GOR-NM-based memory cells read by ΔRH = 30%. The insets of (e) and (f) show sketches of the bending states (bending radius of 5 mm) and the various bending radius (*R*), respectively. g) Schematic illustration of a prototype WORM-chip with 24 pixels (three lines and eight columns), which can be read by human breathing. h) Moisture-powered reading of binary codes and corresponding demodulated display for the word "BIT" according to the ASCII. These data can be reliably stored beyond 30 days.

Just like compact discs (CDs) and digital video disks (DVDs), the WORM-type memory technology is secure for data storage, in which information cannot be modified once written. As a consequence, this technology has attracted considerable research interest and been widely applied as read-only memory in computers to record core data that should be unchangeable (e.g., operating system data).[30] However, the high-performance WORM-type memory requires a high ON/OFF signal ratio, stably repeatable reading process, and nonreproducible writing process.[12,30] In view of these stringent requirements, we fabricated a prototype of the WORM-type memory (**Figure 5**a,b) by pressing a GOR-NM onto an Al substrate with printed Ag top electrode, which showed stable and reversible hydration–dehydration cycles with a remarkably high potential switching ON/OFF ratio (vide infra). Although the direct moisture adsorption of GOR-NM under the top-electrode was hindered by the top electrode, the hydrophility of GOR-NM and the capillarity of its microstructure[24,25] allow the adsorbed water spreading rapidly in the GOR-NM, guaranteeing an expedite hydration. As with the classical WORM-type memory model, the memory function is enabled by an array of single cells, where the cells with GOR-NM and g-GOR-NM (produced by a quick in situ region-specific structural polarization process, Figure S14, Supporting Information) are defined as pristine and written pixels (inset of Figure 5a), serving as OFF and ON states, respectively. As shown in Figure 5c, the moisture-powered voltage signals of written pixels (i.e., g-GOR-NM) were extremely higher than those of pristine pixels (i.e., GOR-NM), and the ON/OFF ratio reaches 10^6 once a ΔRH of about 30% occurs, which is significantly higher than that of conventional resistive switching memory diodes with an ON/OFF ratio of only ≈10^4,[31] indicating a highly depressed misreading risk. More importantly, the potential switching effect for our GOR-NM-based WORM-type memory device depended solely on ΔRH rather than those destructive stimuli, including temperature change, irradiation, applied electric bias, and stress. Thus, the reading cycles for our WORM-type memory device have been stably repeated for more than 1000 times (Figure 5d), demonstrating a highly reliable reading process. Furthermore, the flexible feature of the GOR-NM made the device robust to tolerate the long-term and repeated straight-bending process. As shown in Figure 5 e,f, GOR-NM-based memory cells kept a stable ON/OFF voltage ratio of 10^6 whether they were bended or rolled up into various radius of curvatures over 500 cycles, indicating the excellent stability of our moisture-powered memory devices even under deformation. Since the moisture induced potential switching is based on the preformed switchable ion channels and ionic gradient, the memory effect could, in principle, be retained unless the GOR-based microstructures are fully broken (e.g., being heated to high temperature, as shown in Figure S15,

Supporting Information). Moreover, in contrast to conventional resistive switching memory devices based on current signals, the voltage signal of our GOR-NM-based memory cells did not attenuate with the decreasing pixel size and the functional layer thickness, hence the device size and thickness (Figure S16, Supporting Information), suggesting excellent possibilities to be integrated into miniaturized data recording systems.

Generally speaking, the exhalation of adults through the oral cavity can cause an RH variation of ≈30%. We therefore constructed a GOR-NM-based WORM-chip with 24 bits (8×3 array, also see Figure S17, Supporting Information, for the writing process) to demonstrate a practical application of the self-powered information reading (Figure 5g). As shown in Figure 5h, the voltage signals from the written (i.e., g-GOR-NM) and pristine (i.e., GOR-NM) pixels were demodulated as "1" and "0," respectively, so that a prestored single letter "B" was presented by the eight-bit codes of "01000010" according to the ASCII (American Standard Code for Information Interchange). The other letters of the alphabet can be demodulated similarly (see Figure 5h for "I" and "T" as examples). Therefore, the word "BIT," which is a short name of Beijing Institute of Technology, could be displayed at any time once a person blowing the WORM-chip with his/her mouth, even 30 days after the writing process was performed. Remarkably, all of the abovementioned reading tests were executed without external power supply and there was no cross talk between cells (Figure S18, Supporting Information). Clearly, therefore, a class of novel self-powered memory devices with superb performance has been developed in this study.

As can be seen from above, we have demonstrated that a bioinspired potential switching has been achieved for an artificial structure with moisture enabled switchable ion channels. The moisture switchable ion channels can be produced by dimensionally confined self-assembling GOR-Ns into a layered microporous membrane (GOR-NM), providing expedite moisture diffusion and hydration-dependent ion transport. The ionic gradient is induced by the subsequent structural polarization of GOR-NM by asymmetric electrochemical oxidation/reduction creating gradient oxygen-containing functional groups through the membrane thickness, which makes a gradient concentration distribution of ions generated by self-ionization in response to moisture. These unique properties enable us to devise a class of novel moisture (self)-powered memory devices with excellent performance, as demonstrated by a prototype of GOR-NM-based WORM device to display the word "BIT" with human breath even 30 days after the writing process was performed. Apart from the demonstrated WORM-type information storage, the newly developed GOR-NM-based self-powered moisture responsive chips can be used for many other applications, including breath-based diagnostic biomedical sensors and micro/nanoelectrical generators. Therefore, this work provides a platform technology attractive for a large variety of potential applications.

Supporting Information

Supporting Information is available from the Wiley Online Library or from the author.

Acknowledgements

F.Z. and L.W. contributed equally to this work. The authors thank the financial support from the 973 program of China (2011CB013000) and National Science Fundation of China (21325415, 51673026), and Beijing Natural Science Foundation (2164070, 2152028).

Received: September 15, 2016
Published online: November 14, 2016

[1] D. A. Doyle, J. M. Cabral, R. A. Pfuetzner, A. Kuo, J. M. Gulbis, S. L. Cohen, B. T. Chait, R. MacKinnon, *Science* **1998**, *280*, 69.
[2] D. Ren, B. Navarro, H. X. Xu, L. X. Yue, Q. Shi, D. E. Clapham, *Science* **2001**, *294*, 372.
[3] A. Prindle, J. T. Liu, M. Asally, S. Ly, J. Garcia-Ojalvo, G. M. Süel, *Nature* **2015**, *527*, 59.
[4] M. Ali, S. Nasir, P. Ramirez, I. Ahmed, N. Q. Hung, L. Fruk, S. Mafe, W. Ensinger, *Adv. Funct. Mater.* **2012**, *22*, 390.
[5] Q. Liu, K. Xiao, L. P. Wen, H. Lu, Y. H. Liu, X. Y. Kong, G. H. Xie, Z. Zhang, Z. S. Bo, L. Jiang, *J. Am. Chem. Soc.* **2015**, *137*, 11976.
[6] Y. L. Xu, X. Sui, S. Guan, J. Zhai, L. C. Gao, *Adv. Mater.* **2015**, *27*, 1851.
[7] J. Borghetti, G. S. Snider, P. J. Kuekes, J. J. Yang, D. R. Stewart, R. S. Williams, *Nature* **2010**, *464*, 873.
[8] K. Vanheusden, W. L. Warren, R. A. B. Devine, D. M. Fleetwood, J. R. Schwank, M. R. Shaneyfelt, P. S. Winokur, Z. J. Lemnios, *Nature* **1997**, *386*, 587.
[9] M. Kroutvar, Y. Ducommun, D. Heiss, M. Bichler, D. Schuh, G. Abstreiter, J. J. Finley, *Nature* **2004**, *432*, 81.
[10] S. Möller, C. Perlov, W. Jackson, C. Taussig, S. R. Forrest, *Nature* **2003**, *426*, 166.
[11] M. Ungureanu, R. Zazpe, F. Golmar, P. Stoliar, R. Llopis, F. Casanova, L. E. Hueso, *Adv. Mater.* **2012**, *24*, 2496.
[12] Y. P. Zang, F. J. Zhang, D. Z. Huang, X. K. Gao, C. A. Di, D. B. Zhu, *Nat. Commun.* **2015**, *6*, 1.
[13] F. Zhao, Y. Zhao, H. H. Cheng, L. T. Qu, *Angew. Chem. Int. Ed.* **2015**, *54*, 14951.
[14] S. Kumar, M. D. Pickett, J. P. Strachan, G. Gibson, Y. Nishi, R. S. Williams, *Adv. Mater.* **2013**, *25*, 6128.
[15] H. Wang, F. B. Meng, B. Zhu, W. R. Leow, Y. Q. Liu, X. D. Chen, *Adv. Mater.* **2015**, *27*, 7670.
[16] F. Zhao, Y. Liang, H. H. Cheng, L. Jiang, L. T. Qu, *Energy Environ. Sci.* **2016**, *9*, 912.
[17] F. Zhao, H. H. Cheng, Z. P. Zhang, L. Jiang, L. T. Qu, *Adv. Mater.* **2015**, *27*, 4351.
[18] D. V. Kosynkin, A. L. Higginbotham, A. Sinitskii, J. R. Lomeda, A. Dimiev, B. K. Price, J. M. Tour, *Nature* **2009**, *458*, 872.
[19] S. Deville, *Adv. Eng. Mater.* **2008**, *10*, 155.
[20] W. L. Li, K. Lu, J. Y. Walz, *Int. Mater. Rev.* **2012**, *57*, 37.
[21] Y. Zhao, C. G. Hu, L. Song, L. X. Wang, G. Q. Shi, L. M. Dai, L. T. Qu, *Energy Environ. Sci.* **2014**, *7*, 1913.
[22] C. G. Hu, Y. Zhao, H. H. Cheng, Y. H. Wang, Z. L. Dong, C. C. Jiang, X. Q. Zhai, L. Jiang, L. T. Qu, *Nano Lett.* **2012**, *12*, 5879.
[23] W. Gao, N. Singh, L. Song, Z. Liu, A. L. M. Reddy, L. J. Ci, R. Vajtai, Q. Zhang, B. Q. Wei, P. M. Ajayan, *Nat. Nanotechnol.* **2011**, *6*, 496.
[24] H. Cheng, J. Liu, Y. Zhao, C. Hu, Z. Zhang, N. Chen, L. T. Qu, *Angew. Chem., Int. Ed.* **2013**, *52*, 10482.
[25] H. Cheng, Y. Hu, F. Zhao, Z. Dong, Y. Wang, N. Chen, L. T. Qu, *Adv. Mater.* **2014**, *26*, 2909.
[26] Q. Liu, L. P. Wen, K. Xiao, H. Lu, Z. Zhang, G. H. Xie, X. Y. Kong, Z. S. Bo, L. Jiang, *Adv. Mater.* **2016**, *28*, 3181.

[27] F. Zhao, J. Q. Liu, X. Huang, X. Zou, G. Lu, P. J. Sun, S. X. Wu, W. Ai, M. D. Yi, X. Y. Qi, L. H. Xie, J. L. Wang, H. Zhang, W. Huang, *ACS Nano* **2012**, *6*, 3027.
[28] C. G. Hu, G. P. Zheng, F. Zhao, H. B. Shao, Z. P. Zhang, N. Chen, L. Jiang, L. T. Qu, *Energy Environ. Sci.* **2014**, *7*, 3699.
[29] H. Y. Jeong, J. Y. Kim, J. W. Kim, J. O. Hwang, J. E. Kim, J. Y. Lee, S. Y. Choi, *Nano Lett.* **2010**, *10*, 4381.
[30] J. Q. Liu, Z. Y. Yin, X. H. Cao, F. Zhao, L. H. Wang, W. Huang, H. Zhang, *Adv. Mater.* **2013**, *25*, 233.
[31] C. L. Tan, Z. D. Liu, W. Huang, H. Zhang, *Chem. Soc. Rev.* **2015**, *44*, 2615.